ChemPubSoc Europe

DOI: 10.1002/chem.201500187

CHEMISTRY A European Journal Full Paper

Nickel Complexes

Monometallic Ni^0 and Heterobimetallic Ni^0/Au^I Complexes of Tripodal Phosphine Ligands: Characterization in Solution and in the Solid State and Catalysis

Kyle J. Cluff, Nattamai Bhuvanesh, and Janet Blümel*[a]

Abstract: The tridentate chelate nickel complexes [(CO)Ni{$(PPh_2CH_2)_3CMe$}] (**2**), [(CO)Ni{$(PPh_2CH_2CH_2)_3SiMe$}] (**6**), and [Ph_3PNi{$(PPh_2CH_2CH_2)_3SiMe$}] (**7**), as well as the bidentate complex [$(CO)_2Ni${$(PPh_2CH_2)_2CMeCH_2PPh_2$}] (**3**) and the heterobimetallic complex [$(CO)_2Ni${$(PPh_2CH_2)_2CMeCH_2Ph_2PAuCl$}] (**4**), have been synthesized and fully characterized in solution. All ^1H and ^{13}C NMR signal assignments are based on 2D-NMR methods. Single crystal X-ray structures have been obtained for all complexes. Their ^{31}P CP/MAS (cross polarization with magic angle spinning) NMR spectra have been recorded and the isotropic lines identified. The signals were assigned with the help of their chemical shift anisotropy (CSA) data. All complexes have been tested regarding their catalytic activity for the cyclotrimerization of phenylacetylene. Whereas complexes **2**–**4** display low catalytic activity, complex **7** leads to quantitative conversion of the substrate within four hours and is highly selective throughout the catalytic reaction.

Introduction

The general research interest of our group is to immobilize homogeneous catalysts on insoluble oxide supports, so that the catalyst can easily be separated from the reaction mixtures and recycled.[1,2] The primary remaining problem with both homogeneous and immobilized catalysts is ligand detachment, which leads to leaching and nanoparticle formation. Over the years, realizing that the linkers are crucial for the success of immobilized catalysts, many systems with refined linkers have been obtained, which have shown record activities and lifetimes. These species include rhodium hydrogenation catalysts,[3] Pd^0/Cu^I Sonogashira systems for C–C cross-coupling reactions,[4] and nickel catalysts for acetylene cyclotrimerization[5] and hydrophosphonation.[6]

Nickel catalysts in general merit exploration because they are less expensive than rhodium or palladium catalysts, a factor that is important for large-scale experiments and for industrial applications.[6] In order to blaze a trail for the next generation of immobilized nickel complexes with a new type of linker, molecular analogues are studied in a first step.

The nickel complexes described herein are tested for their catalytic activity with respect to the cyclotrimerization of phenylacetylene. This reaction is important,[7] for example, in natural product syntheses,[7d] and it offers many advantages, including the following: a) The reaction does not require a change of the metal oxidation state, in contrast, for example, to the Sonogashira reaction;[4] b) only one substrate and no base or co-catalyst are needed; c) no gases are involved, as in hydrogenation reactions,[3] and therefore no gas diffusion effects will blur the experimental results; d) there are two isomers as reaction products, which allow for the simultaneous determination of the activity and selectivity; e) the cyclotrimerization reaction proceeds under ambient pressure and at moderate temperatures, and there is already a solid basis of data for comparison.[5]

We have previously demonstrated that one general feature of immobilized catalysts is the potential formation of nanoparticles, which can also lead to an active catalyst, as is the case with rhodium catalysts for hydrogenation.[3a,c] However, in the case of nickel catalysts, nanoparticle formation may lead to less active catalysts, and a nickel mirror at the wall of a Schlenk flask lacks catalytic activity.[5d] Therefore, it is important to use a favorable ligand that shields the metal center from other complexes, thus impeding nanoparticle formation, but still allowing substrate access. With respect to later immobilization it will also become important to shield the metal center from a reactive oxide support surface, which can be accomplished with the right ligands.

Immobilized catalysts that are tethered to oxide supports via bidentate[4a,5a] and tripodal chelating phosphine ligands[3a,c,8] have shown superior recycling characteristics as compared to analogous catalysts bound by monodentate ligands. The retention of the metal center is improved by the increased coordinating strength, as we recently demonstrated by using in situ high-resolution magic angle spinning (HRMAS) NMR spectroscopy.[4a,c] Furthermore, the formation of double layers of linkers,[4a,5c] which enhances metal leaching, cannot occur with tripodal phosphine ligands with only one ethoxysilane group.

Although immobilizable versions of tripodal ligands incorporating ethoxysilane groups[3b,8] or phosphonium salts[3a] can

[a] K. J. Cluff, Dr. N. Bhuvanesh, Prof. J. Blümel
Department of Chemistry, Texas A&M University
College Station, TX, 77842-3012 (USA)
E-mail: bluemel@tamu.edu

easily be synthesized, for the sake of solubility and ease of handling without having to prevent cross-linking, the original tripodal phosphine ligands **1** and **5** (Scheme 1 and Scheme 2) with methyl groups and carbon or silicon as center atoms have been used here. Ligand **5** was chosen because it is closer electronically to the ethoxysilane versions to be considered for later immobilization.[3b,8]

In addition to their potential application as linkers for immobilized catalysts, tripodal phosphine ligands are of fundamental interest in coordination chemistry, due to their potential for dynamic and fluxional ligand scenarios.[9] Furthermore, they might allow the selective synthesis of heterobimetallic complexes[10] that are not only of phenomenological but also practical importance because they might display synergistic effects in catalysis. Heterobimetallic complexes also have the potential to provide metal atom assemblies as preconditioned systems for the formation of nanoparticles with a well-defined stoichiometry of metal atoms.

All complexes in this work have been characterized by solid-state NMR spectroscopy.[11,12] This method grows in importance for the characterization not only of materials like metal–organic frameworks (MOFs), porous organic frameworks (POFs),[13] and polymers,[14] but it is increasingly applied to insoluble molecular metal complexes.[15–17] In this field, solid-state NMR is particularly important, because complexes and ligands might not crystallize readily, and only in some cases are the polycrystalline materials of high enough quality for powder diffraction.[18] Naturally, solid-state NMR spectroscopy is indispensable for investigating immobilized catalysts on amorphous supports such as oxides, which do not allow powder diffraction.[3c] Furthermore, dynamic effects that otherwise complicate the analysis of coordination compounds can be conveniently studied when "frozen" in the solid state.[17]

The spectra presented herein were obtained by using magnetization transfer from protons to ^{31}P nuclei (cross polarization, CP)[11,12] to boost the signal intensities. Magic angle spinning (MAS) was applied to reduce anisotropic line-broadening effects in the solid state.[11]

Besides providing chemical shift information, in favorable cases of clean and polycrystalline materials, solid-state NMR spectra result in a wealth of chemical shift anisotropy (CSA)[12] data. CSA values provide valuable insight about the symmetry of the electronic surroundings of a nucleus, which is of general interest.[16] Most importantly, dynamic processes in molecules[17] and mobilities of adsorbed species on surfaces can be identified and quantified by a reduced or fully eliminated CSA. We could, for example, distinguish polycrystalline from silica-adsorbed metallocenes[19] by their vastly different CSA values, and the interactions of phosphine oxides[20] with silica surfaces and their dynamic behavior could be studied through their CSA data. Finally, from a practical perspective, the CSA is characteristic for each species and thus allows the identification of functional groups in a material or compound. For example, our group has used CSA values to distinguish surface-bound phosphine oxides from phosphonium salts.[21] More recently H_2O_2 adducts of phosphine oxides could be described and distinguished from the corresponding pure phosphine oxides by their characteristic CSA values.[22] Therefore, one of our goals in this contribution is to enlarge the CSA database of nickel phosphine complexes to provide a foundation for further investigation of these catalysts.

Herein we seek to identify a correlation between the X-ray structural, the solid-state NMR, and catalysis results. This combined approach should provide a better insight into the factors that govern acetylene cyclotrimerization catalysis with nickel complexes.

Results and Discussion

The presented results will be outlined according to the following. The starting point is the synthesis of the compounds, followed by the characterization in solution. Then the discussion of the X-ray structures in combination with the solid-state NMR results follows. Finally the complexes will be investigated regarding their catalytic activity.

Syntheses of the nickel complexes

Nickel complex **2** was obtained as a yellow powder in pure form and in high yield from the reaction of the tripodal phosphine ligand **1** with $[Ni(CO)_2(PPh_3)_2]$ in toluene at elevated temperatures (Scheme 1). Alternatively, heating complex **3** to 90 °C for a few hours leads to the quantitative conversion of **3** to **2** (Scheme 1).

An additional option for generating **2** in a straightforward and quantitative manner is to melt complex **3** and thus provoke the loss of one CO group. Complex **3**, in turn, can be obtained selectively and in high yield from the reaction of ligand **1** with $[Ni(CO)_2(PPh_3)_2]$ at ambient temperatures under exclusion of light (Scheme 1). Besides the NMR analysis (see below), the presence of one uncoordinated phosphine group in **3** can be proven by binding it to a gold center (Scheme 1). The colorless heterobimetallic Ni^0/Au^I complex **4** is obtained in a good overall yield of 58%. It has a shelf life of several months at am-

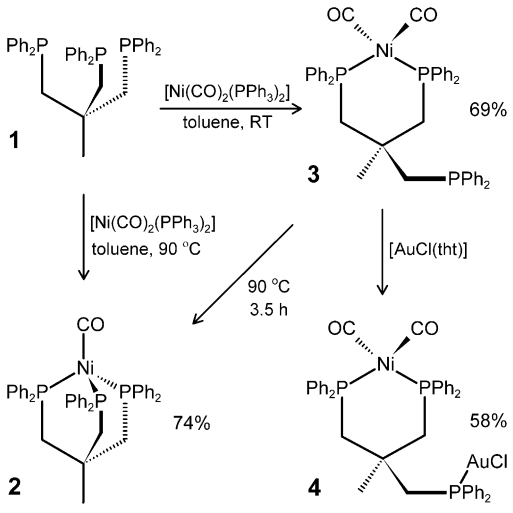

Scheme 1. Syntheses of the monometallic Ni^0 complexes **2** and **3** and of the heterobimetallic Ni^0/Au^I complex **4**. tht = tetrahydrothiophene.

bient temperatures under an inert atmosphere, which is surprising, taking into account that the less noble Ni in an oxidation state of 0 is neighboring an intramolecular Au^{I} center. Decomposition only occurs upon heating **4** up to its melting point. This heterobimetallic Ni^{0}/Au^{I} combination within one molecule is, to our knowledge, unprecedented, although a wealth of Ni^{II}/Au^{I} species have been described.

The tripodal phosphine ligand **5** was synthesized by hydrophosphination using azobisisobutyronitrile (AIBN), as described previously for analogous compounds incorporating ethoxysilane groups.[3b] The nickel complex **6** (Scheme 2) cannot be obtained from the nickel dicarbonyl precursor in an analogous manner to the synthesis of **2** because a multitude of inseparable oligomeric byproducts result from this approach. However, it could be obtained through ligand exchange by the reaction of **5** (Scheme 2) with the monocarbonyl complex $[Ni(CO)(PPh_3)_3]$ cleanly and in a yield of 25%. The synthesis of $[Ni(CO)(PPh_3)_3]$ according to literature procedures proved to be nontrivial.[23] Therefore, we developed a more straightforward synthesis for this complex by making use of a molten mixture of the components $[Ni(CO)_2(PPh_3)_2]$ and PPh_3 in the absence of any solvent. This procedure allowed us to obtain $[Ni(CO)(PPh_3)_3]$ quickly and with a good yield of 62%.

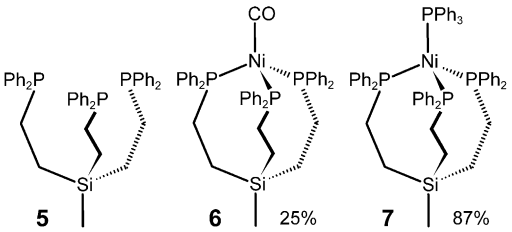

Scheme 2. Structures of the ligand **5** and the Ni^{0} complexes **6** and **7**.

Complex **7** (Scheme 2) could be synthesized by reaction of the Ni^{II} pyridine complex $NiCl_2py_4$ with ligand **5** while offering the corresponding amount of PPh_3 under reducing conditions achieved by adding Zn powder. Hereby, the yield of orange-red **7** was excellent. Additionally, compound **7** is perfectly shelf stable at ambient temperatures over months if kept under an inert atmosphere.

Characterization of the nickel complexes in solution

Due to the symmetries of compounds **1**–**7**, the numbers of NMR signals are small and their signal assignments are straightforward, using signal intensities and coupling patterns. The chemical shifts and coupling constants are in the anticipated ranges for nickel complexes with bidentate[5,15,24] and tripodal phosphine ligands.[3a,8] As in the earlier cases, there is no indication of dynamic processes involving dissociation and recoordination of phosphine groups. Special attention has been given to complex **3** in this respect, but it was found to be static and stable also in solution. Regarding the characterization of the dissolved complexes, the most interesting feature is the occurrence of virtual couplings in the ^{13}C NMR spectra of **2** and **3**.[2,25] These are expected, as we have found and described virtual couplings in tripodal complexes earlier.[2,8]

The assignments of the ^{31}P NMR signals in the spectra of **3**, **4**, and **7** in solution are straightforward due to the signal intensities and $J(^{31}P,^{31}P)$ couplings. All ^{1}H and ^{13}C NMR signal assignments were supported by 2-dimensional NMR methods. For example, the ^{1}H–^{1}H NOESY[26] spectrum of **3** in C_6D_6 proves the signal assignments for the *syn*/*anti* protons in position 3 (Figure 1, solid circle). Only the 3_{anti} proton, which points in the same direction as the methyl protons in position 1, is close enough spatially to give a NOESY cross peak. The 3_{syn} proton *trans* to the methyl group is too far away to give a cross peak (Figure 1, broken line circle).

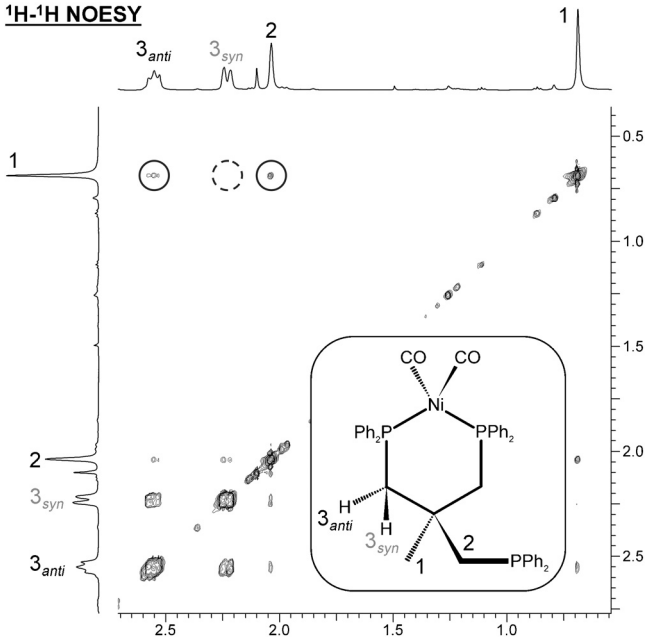

Figure 1. ^{1}H–^{1}H NOESY NMR spectrum of **3** in C_6D_6.

Characterization of the nickel complexes in the solid state

As expected, the IR spectra of the monocarbonyl nickel complexes **2** and **6** show one CO stretching band each in the wavenumber region corresponding to terminal carbonyl groups. The dicarbonyl complexes **3** and **4** display two CO bands each within this region.

Next, the single crystal X-ray analyses of all nickel complexes were evaluated with respect to their corresponding ^{31}P solid-state NMR spectra. The single crystal X-ray structure and unit cell of **2**[27] are shown in Figure 2 and Figure 3, respectively. The ^{31}P CP/MAS spectra of **2** are displayed in Figure 4. The structure shows that the nickel center is tetrahedrally coordinated by the three phosphines of the tripodal ligand and one CO group. The Ni–P bond lengths are 2.182, 2.181, and 2.186 Å, and seem to be mainly dominated by the steric demands of the ligand. The same accounts for the P-Ni-P angles which are smaller than the expected tetrahedral angle and amount to 92.45, 93.91, and 95.95°.[27]

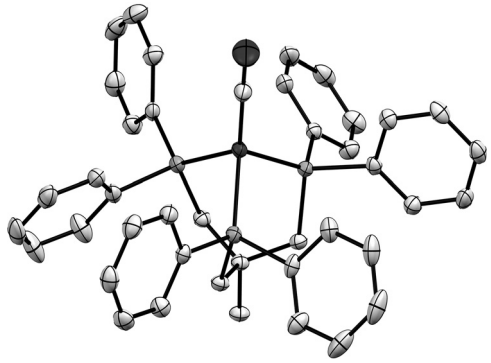

Figure 2. Single crystal X-ray structure of **2**.[27] Thermal ellipsoids are shown at the 50% probability level. Hydrogen atoms are omitted for clarity.

As described above, in solution complex **2** displays only one ^{31}P NMR resonance at 11.54 ppm, due to the symmetry of the molecule. However, in the solid state even this rather spherically shaped complex cannot tumble, but has to assume a fixed position within the lattice. Therefore, the number of ^{31}P solid-state NMR signals is determined by the orientation of the molecules within the unit cell.[11] The maximal number of signals equals the number of magnetically inequivalent ^{31}P nuclei in the unit cell. In the case of similar orientations of functional groups with respect to the external magnetic field, the corresponding lines might overlap, thus reducing the overall number of signals. The CSA parameters[11,12] should reflect the orientation of the functional groups in the unit cell with respect to the external magnetic field. The CSA values are more reliable criteria for making signal assignments in solid-state NMR spectra, because the isotropic chemical shifts can differ substantially from the solution chemical shift values and vary widely, as demonstrated earlier for metal complexes with chelate ligands.[8]

The unit cell of **2** contains four molecules (Figure 3).[27] Hereby, assemblies of two molecules each point in the same direction. Looking along the vertical axis of the unit cell as displayed in Figure 2, one can determine that there should be three ^{31}P NMR signals in the solid-state NMR spectrum. Two phosphine groups have their phenyl substituents pointing downward, whereas one phosphine has them point upward. Therefore, two of the three signals should have similar CSA, whereas that of the third should differ.

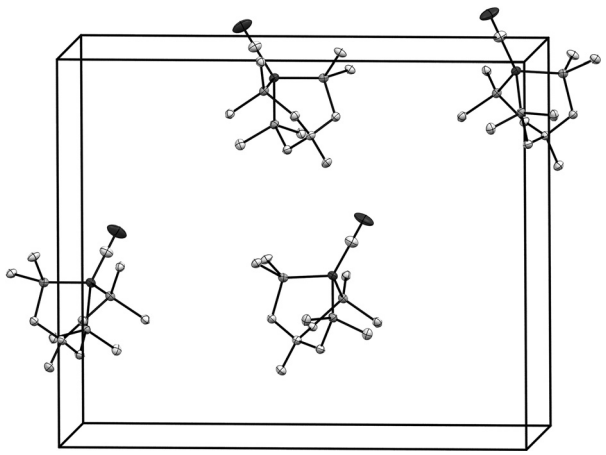

Figure 3. Unit cell of **2**.[27] Thermal ellipsoids are shown at the 50% probability level. Hydrogen atoms and phenyl rings, except for the *ipso* carbons, are omitted for clarity.

Indeed, the solid-state NMR spectra of polycrystalline **2** (Figure 4) can be interpreted in a straightforward manner. Recording the spectra at different rotational speeds of 4 and 7 kHz under optimized Hartmann–Hahn conditions[15] reveals the isotropic lines that do not migrate but retain the same chemical shifts. Three lines can be distinguished and, after deconvolution of the two overlapping isotropic lines and simulation,[28] the CSA data for **2** are obtained.

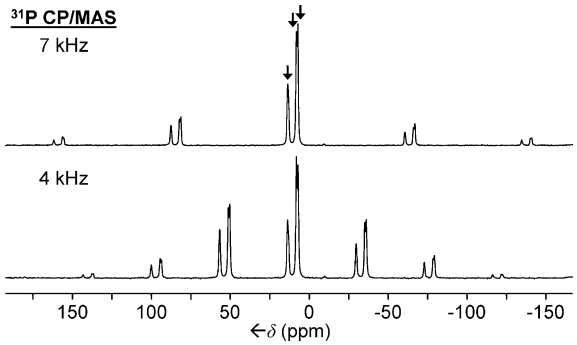

Figure 4. ^{31}P CP/MAS NMR spectra of polycrystalline **2**. Vertical arrows indicate the isotropic lines.

The CSA data of the polycrystalline complexes **2**–**4** and **7** are listed in Table 1. We suggest that the isotropic line at 8.1 ppm corresponds to the phosphine with both its phenyl groups pointing upward in all molecules of the unit cell (Figure 3), because its CSA of 179.5 ppm deviates by more than 20 ppm from the values of the resonance at 13.5 ppm. The difference of the CSA values between the signals at 13.5 and 7.1 ppm is

Table 1. ^{31}P CP/MAS chemical shift anisotropy NMR data [ppm] for the polycrystalline complexes **2**–**4** and **7**.[28]

Complex[a]	δ_{iso}	δ_{11}	δ_{22}	δ_{33}	CSA[b]
2	13.5	107.4	25.6	−92.3	199.7
	8.1	93.9	16.0	−85.6	179.5
	7.1	96.9	19.3	−94.8	191.7
3	16.0	106.4	0.9	−59.4	165.8
	9.6	86.5	17.2	−74.8	161.4
	−31.9	17.8	−47.3	−66.1	83.9
4	19.4	93.2	8.0	−42.9	143.2
	14.1	71.3	29.8	−58.7	130.0
	8.6	74.2	20.6	−69.0	143.2
7	23.6	73.8	68.7	−71.5	145.3
	10.3	79.2	34.6	−83.0	162.3

[a] For structures of complexes, see Schemes 1 and 2; [b] the span of the wideline signals (δ_{11}–δ_{33}) is listed according to the convention described by Duncan.[12]

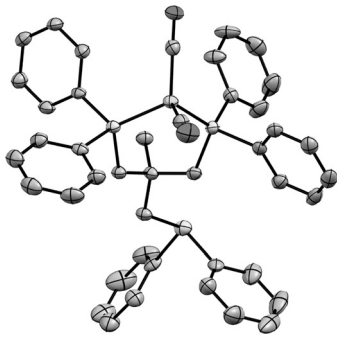

Figure 5. Single crystal X-ray structure of **3**.[29] Thermal ellipsoids are shown at the 50% probability level. Hydrogen atoms are omitted for clarity.

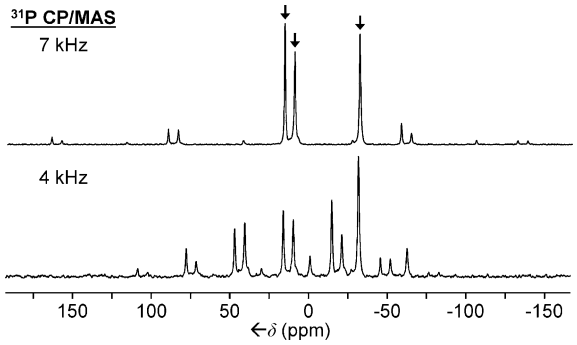

Figure 7. ^{31}P CP/MAS NMR spectra of polycrystalline **3**. Vertical arrows indicate the isotropic lines.

only 8 ppm. Therefore, we assume that these two signals belong to the phosphine groups of **2**, which each have one phenyl group pointing up and one down in the unit cell displayed in Figure 3.

The X-ray structure of **3** shows that only two phosphine groups of the tripodal ligand are coordinated to the nickel center. The third phosphine group remains uncoordinated (Figure 5), although the orientation of its lone pair seems to predestine it to replace one of the two CO groups. The relative stability of **3** might be due to steric constraints of the tripodal ligand and thus hindrance of the attack of the phosphine at the metal center by the *syn*-positioned CO group. Furthermore, the chair conformation of the six-membered ring, which is best seen in the unit cell display (Figure 6), incorporating the nickel atom has to change into a less favorable boat conformation to coordinate the third phosphine group.

The interpretation of the ^{31}P CP/MAS spectra of **3** (Figure 7) is rather straightforward. The resonance at −31.9 ppm corresponds to the uncoordinated phosphine group, because its chemical shift is closest to that found for **3** in solution (−27.79 ppm). Even more indicative, however, is its small CSA value of 83.9 ppm (Table 1). This is in accordance with the fact that the CSA values of phosphines are much smaller than those of their metal-coordinated analogs.[2,4b,12,15] Both the chemical shifts of 9.6 and 16.0 ppm and the CSA values of 165.8 and 161.4 ppm for the other two phosphine resonances are very similar, and therefore, the resonances of the coordinated phosphines cannot be assigned. This is not surprising given the similar orientation of the coordinated phosphine groups as seen in the unit cell of **3**, for example, when looking along the vertical axis in the display (Figure 6).

Interestingly, the X-ray structure of the heterobimetallic complex **4**[30] differs little from that of **3**, except for the additional presence of the AuCl moiety (Figure 8). The unit cell[30] (Figure 9) shows a similar chair conformation of the six-membered ring incorporating the nickel atom. The AuCl moiety is pointed towards the nickel center, with a Ni···Au distance of 7.085 Å. This heterobimetallic complex is rather stable. The

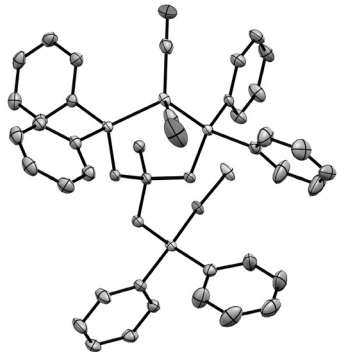

Figure 8. Single crystal X-ray structure of **4**.[30] Thermal ellipsoids are shown at the 50% probability level. Hydrogen atoms are omitted for clarity.

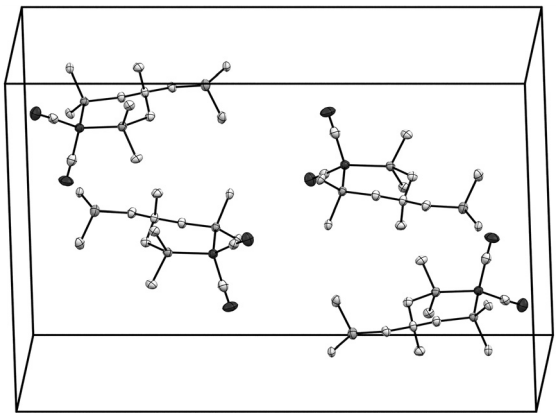

Figure 6. Unit cell of **3**.[29] Thermal ellipsoids are shown at the 50% probability level. Hydrogen atoms and phenyl rings, except for the *ipso* carbons, are omitted for clarity.

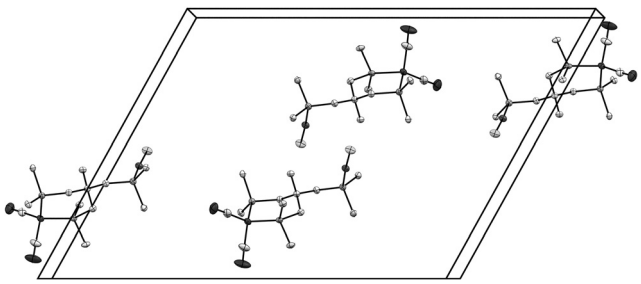

Figure 9. Portion of the unit cell of **4**.[30] Thermal ellipsoids are shown at the 50% probability level. Hydrogen atoms, solvent molecules, and phenyl rings, except for the *ipso* carbons, are omitted for clarity.

steric constraints discussed above for **3** probably also play a major role in **4**.

The packing of complex **4** in the unit cell (Figure 9) again resembles that of **3** (Figure 6). Comparing the ^{31}P CP/MAS spectra of polycrystalline **3** and **4**, the expectation is that the resonance for the uncoordinated phosphine group vanishes and a new signal appears. The signals of the phosphines coordinated to the nickel center should display similar chemical shifts and CSA values.

At first sight, any signal assignment in the ^{31}P CP/MAS spectra of polycrystalline **4** (Figure 10) seems impossible. However,

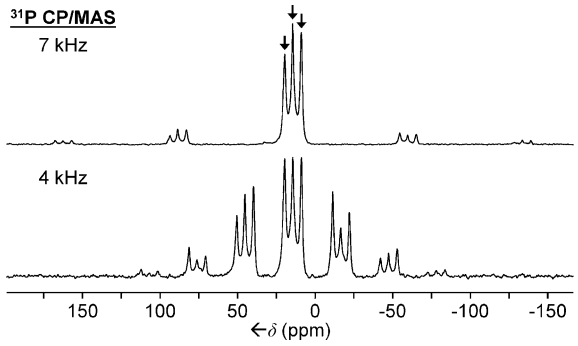

Figure 10. ^{31}P CP/MAS NMR spectra of polycrystalline **4**. Vertical arrows indicate the isotropic lines.

two of the resonances have very similar chemical shifts, 19.4 and 8.6 ppm (Table 1), to those for the nickel-coordinated phosphine groups in **3** (16.0, 9.6 ppm). Furthermore, the CSA values are the same (143.2 ppm) for both resonances. The middle signal at 14.1 ppm has a distinct CSA of only 130.0 ppm. Therefore, we attribute this signal to the phosphine group coordinated to the gold atom in **4**.

Complex **6** has been crystallized from different solvents. The best single crystal X-ray structure of **6**[31] could be solved and it proves the structure in Scheme 2. However, it shows twin crystals and lower quality than the other structures shown herein. Consequently, polycrystalline **6** was not a favorable candidate for solid-state NMR analysis.

Fortunately, complex **7** crystallizes readily and the single crystal analysis resulted in a structure of high quality[32] (Figure 11). It shows that the nickel center is coordinated tetrahedrally by the phosphine atoms, with the P-Ni-P angles of the tripodal ligand assuming the values 107.13, 112.93, and 109.35°. The Ph_3P-Ni-P angles amount to 111.37, 107.42, and 108.46°. Hereby, the phenyl groups of the tripodal ligand shield the metal center from interacting with other nickel complexes, which might inhibit the formation of nickel nanoparticles and premature deactivation of the catalyst, as discussed below. The steric demand of the phenyl groups of the tripodal ligand also interferes with the space occupied by the PPh_3 ligand, which might be the reason for the slightly elongated Ni–PPh_3 bond (2.234 Å) in the molecule, as compared to 2.212, 2.207, and 2.217 Å for the other three Ni–P bond lengths of

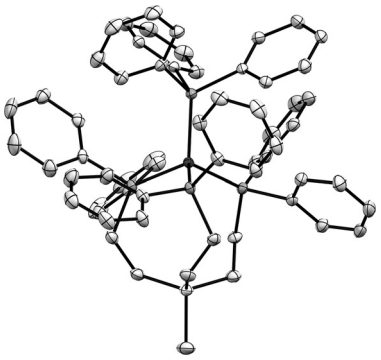

Figure 11. Single crystal X-ray structure of **7**.[32] Thermal ellipsoids are shown at the 50% probability level. Hydrogen atoms are omitted for clarity.

the coordinated tripodal phosphine ligand. This steric factor might indicate a facilitated release of the PPh_3 ligand and thus explain the high catalytic activity of **7**, as discussed below.

Regarding the ^{31}P CP/MAS spectra of polycrystalline **7** (Figure 12), the signal assignment is again straightforward. The

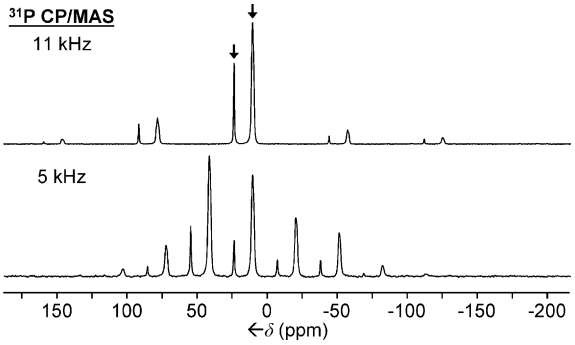

Figure 12. ^{31}P CP/MAS NMR spectra of polycrystalline **7**. Arrows indicate the isotropic lines.

resonances at 23.6 and 10.3 ppm correspond to the phosphine groups of coordinated PPh_3 and tripodal ligand, respectively. This follows from the comparison with the chemical shifts in solution (22.50 and 12.10 ppm) and the signal intensities of about 1:3.5, including the signal intensities of the rotational sidebands. Although, in principle, solid-state NMR signals cannot be integrated when CP is used,[11,15] in the case of **7** it is obvious that there are more alkyl protons close to the phosphine nuclei in the tripodal ligand than in PPh_3. Since alkyl protons facilitate the transfer of magnetization to the phosphorus nuclei, the found ratio of the signal intensities is not exactly 1:3.

As in the cases discussed above, the CSA can be used to additionally corroborate the signal assignment. The electronic surroundings of the ^{31}P nucleus in the PPh_3 ligand is expected to be more symmetric than in the coordinated alkyldiphenylphosphine groups of the tripodal ligand.[21b] Therefore, the CSA value of the PPh_3 signal, 145.3 ppm, is much smaller than that of the tripodal phosphine signal (162.3 ppm, Table 1).

Catalysis

To test the catalytic activity of the nickel complexes shown in Schemes 1 and 2, the cyclotrimerization of phenylacetylene was employed (Scheme 3 and Experimental Section). As described above, the results can readily be compared with a large database of earlier research.[5]

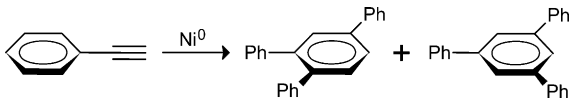

Scheme 3. Nickel-catalyzed cyclotrimerization of phenylacetylene to give the isomers 1,2,4-triphenylbenzene and 1,3,5-triphenylbenzene.

Interestingly, all tripodal phosphine ligands with short alkyl chain lengths [$(CH_2)_1$], namely **2**, **3**, and **4**, displayed only minimal catalytic activities, even at the elevated temperature of 65 °C (Figure 13). One should also note that the presence of Au^I in **4** alongside the Ni^0 center did not lead to a synergistic effect, neither enhancing, nor decreasing the catalytic activity of this heterobimetallic complex.

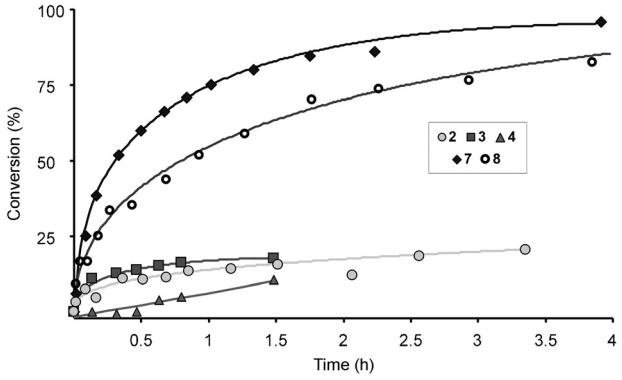

Figure 13. Conversion of phenylacetylene into 1,2,4-triphenylbenzene and 1,3,5-triphenylbenzene at 65 °C in cyclooctane catalyzed by the selected nickel complexes **2**–**4**, **7**, and **8**.

The lower catalytic activities of metal complexes coordinated by ligands with short alkyl chains follows a trend observed earlier for immobilized rhodium hydrogenation catalysts of the Wilkinson type.[3a] At that time the low catalytic activity was attributed to increased decomposition of the catalysts on the reactive silica surface, assuming that the short linker chains do not provide sufficient distance to the support surface. The new results suggest, however, that the coordination of the tripodal ligands might be too strong to allow access of the substrate to the metal center. This general scenario might also explain the low catalytic activity of **2**–**4**. Comparing the IR band for ν(CO) of **2** (1886.5 cm^{-1}) with that of **6** (1911.5 cm^{-1}) corroborates the assumption that the longer alkyl chains of the tripodal ligand **5** render it a poorer electron donor than **1**. Therefore, ligand **5** can more easily liberate the additional coordination site needed for the cyclotrimerization to proceed at the metal center (see below), thus enhancing the catalytic activity.

Indeed, nickel complex **7** leads to nearly quantitative conversion of phenylacetylene into the cyclotrimers within only about four hours. This activity compares very favorably to earlier results, as the highest catalytic activity of a molecular nickel complex reported to date corresponds to a quantitative conversion of the substrate at 90 °C within 4.5 h.[5a] We assume that this high activity, which does not coincide with the formation of a typical nickel mirror at the glass wall of the Schlenk tube, is based on the precarious position of the PPh_3 ligand in **7**. As the X-ray structure[32] (Figure 11) shows, the phenyl groups of the tripodal phosphine ligand are oriented towards the PPh_3 ligand, thus presumably facilitating its departure from the metal center and in this way allowing the substrate to coordinate. To test this hypothesis, the nickel complex [{$CH_3C(CH_2PPh_2)_3$}$NiPPh_3$] (**8**)[33] was applied to the catalytic reaction under identical conditions (Figure 13). As anticipated, **8** is more active than the carbonyl nickel complexes **2**–**4**. However, it does not quite reach the catalytic activity of **7**. In addition to the electronic effects mentioned above, the slightly increased lengths of the alkyl chains of the tripodal ligand in **7** to $(CH_2)_2$ might facilitate further detachment of one or more phosphine groups from the metal center. In order to proceed with the cyclotrimerization reaction, at least two coordination sites have to be liberated at the metal center. However, the ligand detachment seems to be reversible enough to prevent the formation of nickel nanoparticles or a nickel mirror.

The high selectivity of **7** regarding the two possible products (Scheme 3) is unprecedented. Nickel catalysts with mono- and bidentate phosphine ligands studied earlier became unselective during the catalytic run,[5a] producing equal amounts of the two isomers. Catalyst **7**, however, reaches a constant ratio of 1,2,4- to 1,3,5-triphenylbenzene of 16:1 after about 15 min, with an initial product ratio of already 11:1. In comparison, catalyst **8** requires about 30 min to reach a constant ratio of 15:1 with an initial product ratio of 9:1. This scenario shows that, for **7**, the active species is formed most quickly, for example, by releasing the PPh_3 ligand, and that the selectivity is then pushed further towards the product that requires a less sterically demanding transition state.

Putting these results into perspective and comparing the advantages of **7** with those of previously reported catalyst systems is not quite straightforward because each catalyst is usually optimized towards a specific goal. Regarding the selectivity of the unsymmetric versus the symmetric cyclotrimerization products, a [$CoBr_2$(diimine)] complex in combination with Zn and ZnI_2 gave the highest ratio of 97:3.[35] A ruthenium complex was also found to cyclotrimerize phenylacetylene, although 4 mol% of the catalyst had to be applied and the reaction took five hours for completion.[36] A very versatile rhodium complex that is efficient for a variety of terminal and internal acetylenes[37] needs, however, 40 h to produce the cyclotrimers of phenylacetylene with a yield of only 68% in a 1:3 ratio. The most selective catalyst systems for producing the symmetric versus the unsymmetric cyclotrimerization product are based on niobium and tantalum.[38] Isomer ratios of $>$99:1 have been

obtained, but the overall yield was in general lower than 20%. One recent report on the catalytic cyclotrimerization of phenylacetylene describes the activity of a $NiCl_2$/Zn system in the presence of modified pyridines[39] using 20 mol% of catalyst to obtain a yield of 94%. In comparison, only 0.5 mol% of **7** is used and quantitative substrate conversion is achieved within four hours.

In summary, regarding the complexes presented herein, the most promising for future studies on homogeneous and immobilized nickel catalyst systems are complexes with tripodal phosphine ligands of medium length, as realized in **7**, which additionally incorporate a ligand that can be easily detached from the metal center.

Conclusion

In this work, new monometallic Ni^0 complexes and one heterobimetallic Ni^0/Au^I complex with tripodal phosphine ligands have been described. They have been characterized thoroughly in solution and in the solid state. The single crystal X-ray structures of all complexes have been obtained and discussed in connection with their ^{31}P CP/MAS spectra. The CSA values of the complexes have been analyzed and all solid-state NMR signals could be assigned. One nickel complex displayed unprecedented activity and selectivity with respect to the cyclotrimerization of phenylacetylene, which could be interpreted based on the structural features of the complex. The characteristics of this nickel catalyst compare favorably with those of other catalyst systems described in the literature.

Experiments to test the nickel complexes with tripodal phosphine ligands with respect to their catalytic activity in other reactions, for example, as inexpensive substitutes for the Pd component of the Sonogashira reaction, are underway. Furthermore, tripodal phosphine ligands incorporating the ethoxysilane group for immobilized versions of the nickel complexes on oxide supports[3b,8] will be used to transfer the encouraging results on the homogeneous catalysts presented in this paper to the world of catalysts immobilized on oxide supports.

Experimental Section

General remarks

The ^1H, ^{13}C, and ^{31}P NMR spectra of liquids were recorded at 499.70, 125.66, and 202.28 MHz, respectively, on a 500 MHz Varian spectrometer. The ^{13}C and ^{31}P NMR spectra were recorded with ^1H decoupling if not stated otherwise. Neat Ph_2PCl [$\delta(^{31}P) = +81.92$ ppm] in a capillary centered in the 5 mm NMR tubes was used for referencing the ^{31}P chemical shifts of dissolved compounds. For referencing the ^1H and ^{13}C chemical shifts, if not mentioned otherwise, the residual proton signals of the solvent C_6D_6 and the carbon signals were used [$\delta(^1H) = 7.16$ ppm, $\delta(^{13}C) = 128.00$ ppm]. All signal assignments were based on comparisons with analogous metal complexes with tripodal phosphine ligands[3a,b,8] and two-dimensional ^1H–^1H and ^1H–^{13}C correlation spectroscopy. The ^{31}P solid-state NMR spectra were measured with a Bruker Avance 400 widebore NMR spectrometer equipped with a 4 mm multinuclear MAS probehead and ZrO_2 rotors. For the ^{31}P CP/MAS measurements ^1H high-power decoupling was applied with a contact pulse of 5 ms. $NH_4H_2PO_4$ was used to establish the Hartmann–Hahn matching condition and as an external chemical shift standard [$\delta(^{31}P) = +0.81$ ppm]. The recycle delay was 3 s for all CP/MAS spectra. The IR spectra of the neat powders were recorded on a Shimadzu IRAffinity-1 FTIR instrument using a Pike Technologies MIRacle ATR plate. All reactions were carried out using standard Schlenk techniques and a purified N_2 atmosphere, if not stated otherwise. Reagents purchased from Sigma Aldrich or VWR were used without further purification. Tripodal ligand **1** was obtained from Strem Chemicals and used as received. Solvents were dried by boiling them over sodium, then they were distilled and stored under purified nitrogen. Ligand **5** was synthesized according to the procedure described previously.[3b] The ^{31}P and ^{13}C NMR data match those in the literature.[34]

Nickel complex **8** has been obtained by combining $[Ni(cod)_2]$ with the tripodal ligand **1** and PPh_3 at ambient temperature in toluene. The NMR data of **8** are in accordance with those given in the literature.[33]

Representative standardized catalytic procedure using complex **7**: Naphthalene (102.5 mg, 0.7997 mmol) and catalyst **7** (14.0 mg, 0.0140 mmol, 0.5 mol%) were stirred in cyclooctane (5 mL). The mixture was heated to 65 °C and phenylacetylene (0.3 mL, 2.732 mmol) was added via syringe. Single drop aliquots were taken periodically and filtered through a one inch thick layer of silica in a Pasteur pipette and washed with toluene into a GC vial. GC analyses of the catalysis products were obtained with a Shimadzu GC 2010 gas chromatograph equipped with a SHRXI-5 MS column (15 m × 0.25 mm × 0.25 μm) and a flame ionization detector (GC:FID). Naphthalene served as the intensity standard for the GC signals.

Complex **2**: $[Ni(CO)_2(PPh_3)_2]$ (213.8 mg, 0.3344 mmol) and Triphos (208.0 mg, 0.3330 mmol) were dissolved in toluene (50 mL) and stirred at 90 °C for 3.5 h. The solvent was removed from the yellow solution under reduced pressure until solid began to precipitate. Dry pentane (20 mL) was added. The resulting yellow precipitate was filtered, washed with pentane (4 × 20 mL) and dried under vacuum at 70 °C to afford **2** (175.5 mg, 0.2467 mmol, 74% yield with respect to $[Ni(CO)_2(PPh_3)_2]$). Single crystals suitable for X-ray diffraction were obtained from a saturated toluene solution of **2** in the course of a few days. The compound was synthesized previously starting from $[Ni(CO)_4]$,[40] but not characterized with more recent analytical techniques. The complete data are given below.

2

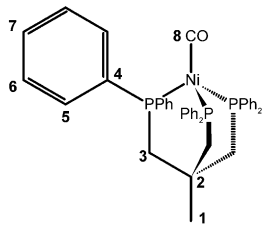

M.p. (decomp.) 158 °C; ^1H NMR (499.69 MHz, C_6D_6): $\delta = 7.50$ (t, 12H, $^3J(^1H,^1H) = 8.3$ Hz, H6), 6.82–6.73 (m, 18H, H5, H7, overlapping), 2.13 (d, 6H, $^2J(^{31}P,^1H) = 7.2$ Hz, H3), 1.22 ppm (q, 3H, $^4J(^{31}P,^1H) = 2.7$ Hz, H1); ^{13}C NMR (125.66 MHz, C_6D_6): $\delta = 207.89$ (q, $^2J(^{31}P,^{13}C) = 4.0$ Hz, C8), 140.62 (virt. m, $^1J(^{31}P,^{13}C) = 42.9$ Hz, C4), 131.93 (d, $^2J(^{31}P,^{13}C) = 16.1$ Hz, C5), 128.29 (s, C7), 127.91 (d, $^3J(^{31}P,^{13}C) = 9.8$ Hz, C6), 38.17 (q, $^2J(^{31}P,^{13}C) = 10.9$ Hz, C2), 36.73 (q, $^3J(^{31}P,^{13}C) = 6.5$ Hz, C1), 36.74–36.53 ppm (virt m, C3); $^{31}P\{^1H\}$ NMR (202.28 MHz, C_6D_6): $\delta = 11.54$ ppm (s); IR: (CO) $\tilde{\nu} = 1886.5$ cm^{-1}.

Complex **3**: Triphos (198.1 mg, 0.3171 mmol) was dissolved in toluene (20 mL) and added to a solution of $[Ni(CO)_2(PPh_3)_2]$ (197.4 mg, 0.3088 mmol) in toluene (22 mL). The mixture was stirred at RT in the dark for 15 h. The solution was concentrated under reduced pressure, resulting in a slightly yellow precipitate, which was filtered off and washed with hexanes (3×10 mL) to give **3** as a white powder (156.3 mg, 0.2114 mmol, 69% yield with respect to $[Ni(CO)_2(PPh_3)_2]$). Single crystals suitable for X-ray diffraction were grown by layering a toluene solution of **3** with pentane.

3

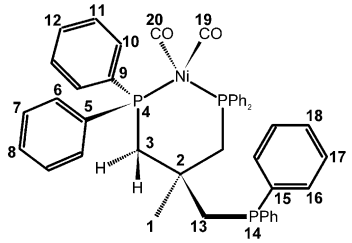

M.p. (quantitative transformation into **2**) 136 °C; ^{1}H NMR (499.69 MHz, C_6D_6): δ = 7.89 (t, 4H, $^3J(^{31}P,^1H)$ = 8.8 Hz, $^3J(^1H,^1H)$ = 7.5 Hz, H10), 7.59 (t, 4H, $^3J(^{31}P,^1H)$ = 8.3 Hz, $^3J(^1H,^1H)$ = 7.5 Hz, H6), 7.35 (t, 4H, $^3J(^{31}P,^1H)$ = 7.3 Hz, $^3J(^1H,^1H)$ = 7.6 Hz, $^4J(^1H,^1H)$ = 1.7 Hz, H16), 7.10–6.92 (m, 18H, H7, H8, H11, H12, H17, H18), 2.56 (dd, 2H, $^2J(^1H,^1H)$ = 14.1 Hz, $^2J(^{31}P,^1H)$ = 11.7 Hz, $H3_{syn}$), 2.23 (dd, 2H, $^2J(^1H,^1H)$ = 14.2 Hz, $^2J(^{31}P,^1H)$ = 3.2 Hz, $H3_{anti}$), 2.04 (dd, 2H, $^4J(^{31}P,^1H)$ = 1.7 Hz, $^2J(^{31}P,^1H)$ = 2.7 Hz, H13), 0.69 ppm (s, 3H, H1); ^{13}C NMR (125.66 MHz, C_6D_6): δ = 202.87 (s, C19), 200.03 (t, $^2J(^{31}P,^{13}C)$ = 3.6 Hz, C20), 140.84 (virt. m, $J(^{31}P,^{13}C)$ = 36.3 Hz, C5*), 140.01 (d, $^1J(^{31}P,^{13}C)$ = 12.7 Hz, C15), 138.93 (virt. m, $J(^{31}P,^{13}C)$ = 30.9 Hz, C9*), 133.40 (d, $^2J(^{31}P,^{13}C)$ = 20.2 Hz, C16), 132.90 (virt. m, $^{2/4}J(^{31}P,^{13}C)$ = 29.1 Hz, C10), 131.78 (virt. m, $^{2/4}J(^{31}P,^{13}C)$ = 28.2 Hz, C6), 129.50 (s, C8$^{\#}$), 128.86 (s, C12$^{\#}$), 128.81–128.70 (m, C17$^{\#}$, C18†), 128.51 (virt. m, $J(^{31}P,^{13}C)$ = 4.5 Hz, C7†, C11†), 49.11 (dt, $^3J(^{31}P,^{13}C)$ = 8.5 Hz, $^1J(^{31}P,^{13}C)$ = 17.5 Hz, C13), 40.71 (ddd, $^3J(^{31}P,^{13}C)$ = 8.6 Hz, $^3J(^{31}P,^{13}C)$ = 8.0 Hz, $^1J(^{31}P,^{13}C)$ = 11.3 Hz, C3), 39.09 (dt, $^2J(^{31}P,^{13}C)$ = 13.6 Hz, $^2J(^{31}P,^{13}C)$ = 4.7 Hz, C2), 29.29 ppm (dt, $^3J(^{31}P,^{13}C)$ = 10.0 Hz, $^3J(^{31}P,^{13}C)$ = 6.4 Hz, C1); *,$^{\#}$,† assignments interchangeable; $^{31}P\{^1H\}$ NMR (202.28 MHz, C_6D_6): δ = 13.93 (d, 2P, $^4J(^{31}P,^{31}P)$ = 2.2 Hz, P4), −27.79 ppm (t, 1P, $^4J(^{31}P,^{31}P)$ = 2.2 Hz, P14); IR: (CO) = $\tilde{\nu}$ = 1998.3, 1931.8 cm^{-1}.

Complex **4**: [AuCl(tht)] (19.0 mg, 0.0593 mmol; tht = tetrahydrothiophene) was added to a solution of **3** (45.9 mg, 0.0621 mmol) in toluene (10 mL). The solution immediately assumed a dark purple color. After stirring the reaction mixture for 20 h, the solvent was removed under reduced pressure, yielding a purple solid. The solid was triturated in ether (50 mL), stirred briefly, and allowed to settle overnight. The clear supernatant solution was then collected and concentrated under reduced pressure. The residue was then re-dissolved in THF (2 mL) and the product precipitated as a white powder when pentane (40 mL) was added. The solid was washed with pentane (1×10 mL) to yield pure **4** as a white powder (33.1 mg, 58% yield with respect to [AuCl(tht)]). Single crystals suitable for X-ray diffraction analysis were grown by slow diffusion of liquid pentane into a THF solution of **4**.

4

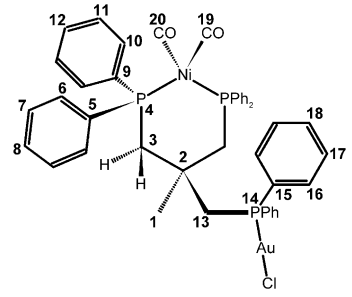

M.p. (decomp.) 133 °C; ^{1}H NMR (499.69 MHz, C_6D_6): δ = 7.85 (dd, 8H, $^3J(^1H,^1H)$ = 7.6 Hz, $^3J(^{31}P,^1H)$ = 9.2 Hz, H6, H10), 7.14 (tm, 4H, $^3J(^1H,^1H)$ = 7.8 Hz, H7), 7.10 (tm, 4H, $^3J(^1H,^1H)$ = 7.8 Hz, H11), 7.06 (ddt, 4H, $^3J(^{31}P,^1H)$ = 12.8 Hz, $^3J(^1H,^1H)$ = 7.1 Hz, $^4J(^1H,^1H)$ = 1.5 Hz, H16), 7.00 (dtt, 2H, $^5J(^{31}P,^1H)$ = 1.2 Hz, $^3J(^1H,^1H)$ = 7.4 Hz, $^4J(^1H,^1H)$ = 1.2 Hz, H8), 6.92 (dtt, 2H, $^5J(^{31}P,^1H)$ = 1.2 Hz, $^3J(^1H,^1H)$ = 7.4 Hz, $^4J(^1H,^1H)$ = 1.2 Hz, H12), 6.89 (dtt, 2H, $^5J(^{31}P,^1H)$ = 2.1 Hz, $^3J(^1H,^1H)$ = 7.4 Hz, $^4J(^1H,^1H)$ = 1.6 Hz, H18), 6.82 (dtt, 4H, $^4J(^{31}P,^1H)$ = 2.4 Hz, $^3J(^1H,^1H)$ = 7.5 Hz, $^4J(^1H,^1H)$ = 1.5 Hz, H17), 2.68 (dd, 2H, $^2J(^{31}P,^1H)$ = 8.2 Hz, $^2J(^1H,^1H)$ = 14.2 Hz, $H3_{syn}$), 2.27 (dd, 2H, $^2J(^{31}P,^1H)$ = 6.7 Hz, $^2J(^1H,^1H)$ = 14.2 Hz, $H3_{anti}$), 2.01 (d, 2H, $^2J(^{31}P,^1H)$ = 11.5 Hz, H13), 0.74 ppm (s, 3H, H1); $^{13}C\{^1H,^{31}P\}$ NMR (125.66 MHz, C_6D_6): δ = 201.25 (s, C19), 201.03 (s, C20), 139.09 (s, C5, C9), 134.16 (s, C15), 133.35 (s, C16), 132.92 (s, C10), 132.35 (s, C6), 131.40 (s, C18), 129.56 (s, C8), 129.43 (s, C12), 129.12 (s, C17), 128.88 (s, C11), 128.72 (s, C7), 43.06 (s, C13), 41.06 (s, C3), 38.67 (s, C2), 31.76 ppm (s, C1); $^{31}P\{^1H\}$ NMR (202.28 MHz, C_6D_6): δ = 14.04 (d, 2P, $^4J(^{31}P,^{31}P)$ = 1.3 Hz, P4), 16.20 ppm (m, 1P, P14); IR: (CO) $\tilde{\nu}$ = 1999.3, 1933.7 cm^{-1}.

$[Ni(CO)(PPh_3)_3]$: $[Ni(CO)(PPh_3)_3]$ was prepared by stirring a blend of molten $[Ni(CO)_2(PPh_3)_2]$ (131.7 mg, 0.2060 mmol) and PPh_3 (0.9976 g, 3.8034 mmol) at 160 °C for 40 min while a slow stream of N_2 was passed over the mixture. The resulting bright yellow liquid was allowed to cool, but not enough to solidify (ca. 100 °C), and dry pentane (10 mL) was added and the mixture shaken causing a precipitate to form. The latter was washed with pentane (4× 10 mL) and then dried under vacuum to give the product as a bright yellow powder (111.7 mg, 0.1279 mmol, 62% yield). The ^{31}P NMR chemical shift matches the literature values.[23c,d] ^{1}H NMR (499.69 MHz, C_6D_6): δ = 7.36 (bdd, 2H, $^3J(^1H,^1H)$ = 7.36 Hz, $^3J(^{31}P,^1H)$ = 7.36 Hz, H_o), 6.95 (t, 1H, $^3J(^1H,^1H)$ = 7.38 Hz, H_p), 6.84 ppm (t, 2H, $^3J(^1H,^1H)$ = 7.49 Hz, H_m); ^{13}C NMR (125.66 MHz, C_6D_6): δ = 201.25 (q, $^2J(^{31}P,^{13}C)$ = 6.61 Hz, *C*O), 139.15 (virt. m, $^1J(^{31}P,^{13}C)$ = 34.6 Hz, C_i), 134.09 (dd, $^4J(^{31}P,^{13}C)$ = 4.9 Hz, $^2J(^{31}P,^{13}C)$ = 9.08 Hz, C_o), 128.35 (s, C_p), 127.87 ppm (dd, $^5J(^{31}P,^{13}C)$ = 2.9 Hz, $^3J(^{31}P,^{13}C)$ = 5.58 Hz, C_m); $^{31}P\{^1H\}$ NMR (202.28 MHz, C_6D_6): δ = 31.90 ppm.

Complex **6**: $[Ni(CO)(PPh_3)_3]$ (0.1117 g, 0.1279 mmol) was dissolved in toluene (10 mL) and combined with a solution of **5** (87.2 mg, 0.1277 mmol) in toluene (10 mL). This mixture was stirred for 75 min, after which the solvent was removed under reduced pressure. The resulting solid was washed with pentane (3×10 mL), dissolved in toluene (3 mL), and precipitated by adding pentane (2× 10 mL). The resulting yellow powder was shown by ^{31}P NMR spectroscopy to contain **6** (34.5 mg, 0.0448 mmol, 25% yield), alongside a small amount of PPh_3, and presumably oligomeric side products. These impurities were removed by repeated precipitation from a toluene solution by pentane. Crystals suitable for X-ray diffraction were obtained by slow diffusion of liquid pentane into a toluene solution of **6**.

M.p. (decomp.) 113 °C; $^1H\{^{31}P\}$ NMR (499.69 MHz, C_6D_6): δ = −0.06 (s, 3H, H1), 0.74 (m, 6H, H2), 2.15 (m, 6H, H3), 6.95–6.99 (m, 18H, H6, H8), 7.47–7.50 ppm (m, 12H, H7); $^{13}C\{^{31}P,^1H\}$ NMR (125.66 MHz, $[D_8]$THF, $\delta(^{13}C)$ = 25.37): δ = 142.41 (C5), 132.35 (C6), 128.55 (C7), 128.31 (C8), 23.73 (C3), 8.40 (C2), 5.79 ppm (C1); $^{31}P\{^1H\}$ NMR

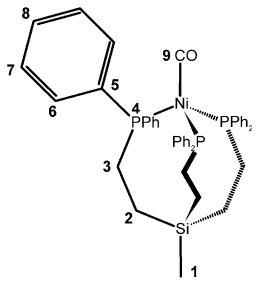

6

(202.28 MHz, toluene): $\delta = 19.81$ ppm (s, P4); IR: (CO) $\tilde{\nu} = 1911.5\ cm^{-1}$.

Complex **7**: $[NiCl_2py_4]$ (103.8 mg, 0.2327 mmol) and ligand **5** (157.7 mg, 0.2309 mmol) were stirred in THF (40 mL). The opaque reaction mixture turned red immediately and then the color faded to white within 1 min. Subsequently, PPh_3 (62.6 mg, 0.239 mmol) was added, followed by Zn powder (2.000 g, 30.58 mmol). The reaction mixture was degassed under vacuum for 2 min and then stirred for 16 h. During this time a clear, orange-red solution formed alongside solid matter. After settling, the solution was separated from the precipitate via syringe and the solvent was removed under reduced pressure. The resulting residue was extracted by stirring with toluene. The solids were allowed to settle and the supernatant was collected, stripped of the solvent, and the residue was washed with pentane (10 mL) and dried under vacuum, giving the product as an orange-red powder (203.4 mg, 0.2026 mmol, 87% yield).

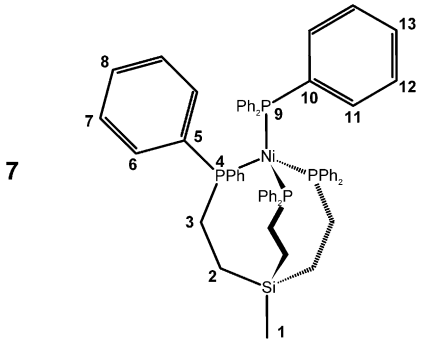

7

M.p. (decomp.) 38 °C; ^1H NMR (499.69 MHz, C_6D_6): $\delta = -0.25$ (s, 3H, H1), 0.70 (bs, 6H, H2), 2.43 (vbs, 6H, H3), 6.58 (dd, 6H, $^3J(^{31}P,^1H) = 7.6$ Hz, $^3J(^1H,^1H) = 7.0$ Hz, H11), 6.81 (t, 6H, $^3J(^1H,^1H) = 7.2$ Hz, H12), 6.89 (t, 3H, $^3J(^1H,^1H) = 7.1$ Hz, H13), 7.11 (bs, 24H, H6, H7), 7.30 ppm (bs, 6H, H8); $^{13}C\{^{31}P,^1H\}$ NMR (125.66 MHz, $[D_8]$THF, $\delta(^{13}C) = 25.37$): $\delta = 5.18$ (s, C1), 9.02 (s, C2), 27.82 (s, C3), 141.04 (s, C5), 149.86 (s, C10), 134.82 (s, C11), 134.17 (bs, C6), 129.10 (s, C8), 128.21 (s, C13), 128.03 (s, C7), 127.81 ppm (s, C12); $^{31}P\{^1H\}$ NMR (202.28 MHz, C_6D_6): $\delta = 12.01$ (d, 3P, $^2J(^{31}P,^{31}P) = 18.1$ Hz, P4), 22.50 ppm (q, 1P, $^2J(^{31}P,^{31}P) = 18.2$ Hz, P9).

Acknowledgements

This work was supported by the Robert A. Welch Foundation (A-1706), the National Science Foundation (CHE-0911207, CHE-1300208, CHE-0840464), and the *APPEAL* Consortium at Texas A&M University.

Keywords: homogeneous catalysis · nickel · NMR spectroscopy · phosphane ligands · solid-state structures

[1] a) *Heterogenized Homogeneous Catalysts for Fine Chemicals Production* (Eds.: P. Barbaro, F. Liguori), Springer, Heidelberg, **2010**; b) *Chiral Catalyst Immobilization and Recycling* (Eds.: D. E. De Vos, I. F. J. Vankelecom, P. A. Jacobs), Wiley-VCH, Weinheim, **2000**; c) G. Rothenberg, *Catalysis: Concepts and Green Applications*, Wiley-VCH, Weinheim, **2008**.

[2] J. Blümel, *Coord. Chem. Rev.* **2008**, *252*, 2410 – 2423.

[3] a) J. Guenther, J. Reibenspies, J. Blümel, *Adv. Synth. Catal.* **2011**, *353*, 443 – 460; b) J. Guenther, N. Bhuvanesh, J. Blümel, unpublished results; c) R. Silbernagel, A. Diaz, E. Steffensmeier, A. Clearfield, J. Blümel, *J. Mol. Catal. A* **2014**, *394*, 217 – 223; d) C. Merckle, J. Blümel, *Adv. Synth. Catal.* **2003**, *345*, 584 – 588; e) C. Merckle, J. Blümel, *Top. Catal.* **2005**, *34*, 5 – 15; f) Y. Yang, B. Beele, J. Blümel, *J. Am. Chem. Soc.* **2008**, *130*, 3771 – 3773; g) B. Beele, J. Guenther, M. Perera, M. Stach, T. Oeser, J. Blümel, *New J. Chem.* **2010**, *34*, 2729 – 2731.

[4] a) J. C. Pope, T. Posset, N. Bhuvanesh, J. Blümel, *Organometallics* **2014**, *33*, 6750 – 6753; b) T. Posset, J. Blümel, *J. Am. Chem. Soc.* **2006**, *128*, 8394 – 8395; c) T. Posset, J. Guenther, J. Pope, T. Oeser, J. Blümel, *Chem. Commun.* **2011**, *47*, 2059 – 2061.

[5] a) S. Reinhard, P. Soba, F. Rominger, J. Blümel, *Adv. Synth. Catal.* **2003**, *345*, 589 – 602; b) S. Reinhard, K. D. Behringer, J. Blümel, *New J. Chem.* **2003**, *27*, 776 – 778; c) K. D. Behringer, J. Blümel, *Chem. Commun.* **1996**, 653 – 654; d) T. Posset, Dissertation Thesis, University of Heidelberg, **2006**.

[6] a) P. Kumar, J. Louie in *Transition-Metal-Mediated Aromatic Ring Construction* (Ed.: K. Tanaka), Wiley, Hoboken, **2013**, pp. 37 – 70; b) M. C. Biel, R. Kessinger, J. Sommer, J. Blümel, U.S. Patent, 8318968 B2, **2012**; [*Chem. Abstr.* **2012**, *2008*, 1157541]; c) M. C. Biel, R. Kessinger, J. Sommer, J. Blümel, U.S. Patent, WO 2008113777, **2008**; [*Chem. Abstr.* **2008**, *149*, 402503].

[7] a) D. L. J. Broere, E. Ruijter, *Synthesis* **2012**, 2639 – 2672; b) R. Hua, M. V. A. Abrenica, P. Wang, *Curr. Org. Chem.* **2011**, *15*, 712 – 729; c) Y. Shibata, K. Tanaka, *Synthesis* **2012**, 323 – 350; d) G. Domínguez, J. Perez-Castells, *Chem. Soc. Rev.* **2011**, *40*, 3430 – 3444.

[8] M. Bogza, T. Oeser, J. Blümel, *J. Organomet. Chem.* **2005**, *690*, 3383 – 3389.

[9] Selected references: a) R. Gilbert-Wilson, L. D. Field, M. M. Bhadbhade, *Inorg. Chem.* **2012**, *51*, 3239 – 3246; b) P. J. Desrochers, D. S. Duong, A. S. Marshall, S. A. Lelievre, B. Hong, J. R. Brown, R. M. Tarkka, J. M. Manion, G. Holman, J. W. Merkert, D. A. Vicic, *Inorg. Chem.* **2007**, *46*, 9221 – 9233; c) R. B. Bedford, M. Betham, C. P. Butts, S. J. Coles, M. Cutajar, T. Gelbrich, M. B. Hursthouse, P. N. Scully, S. Wimperis, *Dalton Trans.* **2007**, 459 – 466; d) C. E. MacBeth, J. C. Thomas, T. A. Betley, J. C. Peters, *Inorg. Chem.* **2004**, *43*, 4645 – 4662.

[10] Selected recent references: a) D. Fernández-Anca, M. I. Garcia-Seijo, M. E. Garcia-Fernandez, *Dalton Trans.* **2010**, *39*, 2327 – 2336; b) D. Fernández-Anca, M. I. Garcia-Seijo, A. Castineiras, M. E. Garcia-Fernandez, *Inorg. Chem.* **2008**, *47*, 5685 – 5695; c) A. B. Chaplin, Z. Beni, C. G. Hartinger, H. H. Ben, A. D. Phillips, R. Scopelliti, P. J. Dyson, *J. Cluster Sci.* **2008**, *19*, 295 – 309; d) P. W. Miller, A. J. P. White, *J. Organomet. Chem.* **2010**, *695*, 1138 – 1145.

[11] C. A. Fyfe, *Solid-State NMR for Chemists*, CFC Press, Guelph, ON, **1983**.

[12] T. M. Duncan, *A Compilation of Chemical Shift Anisotropies*, Farragut Press, Chicago, IL, **1990**.

[13] W. Lu, D. Yuan, D. Zhao, C. I. Schilling, O. Plietzsch, T. Muller, S. Bräse, J. Guenther, J. Blümel, R. Krishna, Z. Li, H.-C. Zhou, *Chem. Mater.* **2010**, *22*, 5964 – 5972.

[14] a) J. C. Pope, H.-J. Sue, T. Bremner, J. Blümel, *Polymer* **2014**, *55*, 4577 – 4585; b) J. C. Pope, H.-J. Sue, T. Bremner, J. Blümel, *J. Appl. Polym. Sci.* **2015**, *132*, 1804 – 1816; c) J. Guenther, M. Wong, H.-J. Sue, T. Bremner, J. Blümel, *J. Appl. Polym. Sci.* **2013**, *128*, 4395 – 4404.

[15] S. Reinhard, J. Blümel, *Magn. Reson. Chem.* **2003**, *41*, 406 – 416.

[16] a) J. W. Diesveld, E. M. Menger, H. T. Edzes, W. S. Veeman, *J. Am. Chem. Soc.* **1980**, *102*, 7935 – 7936; b) K. Eichele, R. E. Wasylishen, J. F. Corrigan, N. J. Taylor, A. J. Carty, K. W. Feindel, G. M. Bernard, *J. Am. Chem. Soc.* **2002**, *124*, 1541 – 1552.

[17] M. R. Chierotti, R. Gobetto, *Eur. J. Inorg. Chem.* **2009**, 2581 – 2597.

[18] N. Masciocchi, S. Galli, M. Bogza, J. Blümel, *Powder Diffr.* **2007**, *22*, 55 – 58.
[19] a) K. J. Cluff, N. Bhuvanesh, J. Blümel, *Organometallics* **2014**, *33*, 2671 – 2680; b) K. J. Cluff, M. Schnellbach, C. R. Hilliard, J. Blümel, *J. Organomet. Chem.* **2013**, *744*, 119 – 124.
[20] C. R. Hilliard, S. Kharel, K. J. Cluff, J. A. Gladysz, J. Blümel, *Chem. Eur. J.* **2014**, *20*, 17292 – 17295.
[21] a) J. Blümel, *Inorg. Chem.* **1994**, *33*, 5050 – 5056; b) J. Sommer, Y. Yang, D. Rambow, J. Blümel, *Inorg. Chem.* **2004**, *43*, 7561 – 7563.
[22] C. R. Hilliard, N. Bhuvanesh, J. A. Gladysz, J. Blümel, *Dalton Trans.* **2012**, *41*, 1742 – 1754.
[23] Selected more recent references: a) T. Yamamoto, J. Ishizu, T. Kohara, S. Komiya, A. Yamamoto, *J. Am. Chem. Soc.* **1980**, *102*, 3758 – 3764; b) S. Gambarotta, C. Floriani, A. Chiesi-Villa, C. Guastini, *Organometallics* **1986**, *5*, 2425 – 2433; c) T. R. Gaffney, J. A. Ibers, *Inorg. Chem.* **1982**, *21*, 2860 – 2864; d) L. S. Isaeva, L. N. Morozova, D. N. Kravtsov, *Inorg. Chim. Acta* **1990**, *171*, 29 – 33.
[24] F. Piestert, R. Fetouaki, M. Bogza, T. Oeser, J. Blümel, *Chem. Commun.* **2005**, 1481 – 1483.
[25] a) W. H. Hersh, P. Xu, B. Wag, J. W. Yom, C. K. Simpson, *Inorg. Chem.* **1996**, *35*, 5453 – 5459; b) W. H. Hersh, *J. Chem. Educ.* **1997**, *74*, 1485 – 1488.
[26] S. Brenna, T. Posset, J. Furrer, J. Blümel, *Chem. Eur. J.* **2006**, *12*, 2880 – 2888.
[27] CCDC 1037015 (**2**) contains the supplementary crystallographic data for this paper. These data can be obtained free of charge from The Cambridge Crystallographic Data Centre via www.ccdc.cam.ac.uk/data_request/cif. $C_{42}H_{39}NiOP_3$; unit cell parameters: *a* 17.94920.564(5), *b* 10.117(3), *c* 16.976(5); *Pna*2_1.
[28] Program "dmfit": D. Massiot, F. Fayon, M. Capron, I. King, C. S. Le, B. Alonso, J.-O. Durand, B. Bujoli, Z. Gan, G. Hoatson, *Magn. Reson. Chem.* **2002**, *40*, 70 – 76.
[29] CCDC 1037016 (**3**) contains the supplementary crystallographic data for this paper. These data can be obtained free of charge from The Cambridge Crystallographic Data Centre via www.ccdc.cam.ac.uk/data_request/cif. $C_{43}H_{39}NiO_2P_3$; unit cell parameters: *a* 8.5795(12), *b* 24.844(3), *c* 17.483(3); $P2_1/n$.
[30] CCDC 1037017 (**4**) contains the supplementary crystallographic data for this paper. These data can be obtained free of charge from The Cambridge Crystallographic Data Centre via www.ccdc.cam.ac.uk/data_request/cif. $C_{43}H_{39}AuClNiO_2P_3$, 0.9(C_4H_8O), 0.1(H_2O), unit cell parameters: *a* 38.030(3), *b* 11.0474(8), *c* 25.887(2); *C2/c*.
[31] CCDC 1039467 (**6**) contains the supplementary crystallographic data for this paper. These data can be obtained free of charge from The Cambridge Crystallographic Data Centre via www.ccdc.cam.ac.uk/data_request/cif. $C_{44}H_{45}NiP_3Si$; unit cell parameters: *a* 10.465(2), *b* 10.485(2), *c* 18.592(4); $P2_1/n$.
[32] CCDC 1037018 (**7**) contains the supplementary crystallographic data for this paper. These data can be obtained free of charge from The Cambridge Crystallographic Data Centre via www.ccdc.cam.ac.uk/data_request/cif. $C_{61}H_{60}NiP_4Si$; 0.72(C_5H_{12}), 0.28(C_3H_7), 0.28(C_2H_5), unit cell parameters: *a* 13.2287(11), *b* 16.4601(14), *c* 13.7514(12); $P2_1$.
[33] J. Mautz, K. Heinze, H. Wadepohl, G. Huttner, *Eur. J. Inorg. Chem.* **2008**, 1413 – 1422.
[34] D. E. Hendriksen, A. A. Oswald, G. B. Ansell, S. Leta, R. V. Kastrup, *Organometallics* **1989**, *8*, 1153 – 1173.
[35] G. Hilt, T. Vogler, W. Hess, F. Galbiati, *Chem. Commun.* **2005**, 1474 – 1475.
[36] B. O. Öztürk, S. Karabulut, Y. Imamoglu, *Appl. Catal. A Gen.* **2012**, *433 – 434*, 214 – 222.
[37] V. P. Anju, D. K. Roy, R. S. Anju, S. Ghosh, *J. Organomet. Chem.* **2013**, *733*, 79 – 81.
[38] M. Matsuura, T. Fujihara, M. Kakeya, T. Sugaya, A. Nagasawa, *J. Organomet. Chem.* **2013**, *745 – 746*, 288 – 298.
[39] C. Xi, Z. Sun, Y. Liu, *Dalton Trans.* **2013**, *42*, 13327 – 13330.
[40] J. Chatt, F. A. Hart, *J. Chem. Soc.* **1965**, 812 – 813.

Received: January 15, 2015
Revised: April 23, 2015
Published online on June 8, 2015